South African extreme weather during the 1877–1878 El Niño

Weather – October 2023, Vol. 78, No. 10

Yuri Brugnara[1,2], Stefan Brönnimann[1,2], Stefan Grab[3], Jessica Steinkopf[3,4], Angela-Maria Burgdorf[1,2], Clive Wilkinson[5] and Rob Allan[6]

[1]*Institute of Geography, University of Bern, Switzerland*
[2]*Oeschger Centre for Climate Change Research, University of Bern, Switzerland*
[3]*School of Geography, Archaeology and Environmental Studies, University of the Witwatersrand, Johannesburg, South Africa*
[4]*Global Change Institute, University of the Witwatersrand, Johannesburg, South Africa*
[5]*Climatic Research Unit, University of East Anglia, Norwich, UK*
[6]*Met Office Hadley Centre, Exeter, UK*

Introduction

The period 1877–1878 has been described as the 'Global Famine' (Davis, 2001; Singh *et al.*, 2018), 'Great Drought' (Singh *et al.*, 2018) or 'Global Drought' (Hao *et al.*, 2010) and is associated with the well-known major El Niño event at this time (Huang *et al.*, 2020). During an El Niño, major atmospheric circulation changes take place, resulting in many regional weather and climate anomalies with subsequent socio-economic impacts (e.g. Nicholson and Kim, 1997; Aceituno *et al.*, 2009). During the 1877–1878 event, severe drought occurred in parts of India, China, Indonesia, the Philippines, the Americas, Africa, Australia and the Mediterranean (Aceituno *et al.*, 2009; Singh *et al.*, 2018). It was estimated that 15–25 million people in India and northern China died from drought-related diseases and famine between 1876 and 1879 (Davis, 2001). Conversely, some regions (e.g. parts of the US and northwestern South America) experienced exceptionally wet conditions (e.g. Kiladis and Diaz, 1986; Aceituno *et al.*, 2009; Singh *et al.*, 2018). The period 1877–1878 is thus not one of 'global drought', but perhaps better described as one of 'global extremes in its hydro-climate'.

One of the best examples of strongly contrasting rainfall conditions during this time is evident from westernmost and central/eastern regions of South Africa. Although 1877–1878 is described as a 'great drought' in South Africa, 1878 is identified as the wettest year in the 176 year instrumental rain record for Cape Town (Ndebele *et al.*, 2020). Specifically, the summer rainfall zone (SRZ, covering the interior and eastern regions of South Africa) and the winter rainfall zone (WRZ, covering the southwestern Cape region of South Africa), recorded dry and wet conditions, respectively, during the mid-late 1870s (Vogel, 1989; Nash, 2017; Nash *et al.*, 2019).

A limitation for this time period has been the availability of daily instrumental weather records, as most have a monthly or annual resolution at best. To study daily-scale variability, we require instrumental measurements that are in large part not available in machine-readable format. Here, we show how the digitisation of a relatively small amount of ship-based measurements can improve our ability to reconstruct the weather of South Africa during 1877–1878.

Data

We digitised sub-daily air temperature, sea-surface temperature and air pressure measurements made by 21 British ships sailing mainly between the Atlantic and the Indian Ocean during 1876–1878 (*c.* 15 000

Table 1

List of the newly digitised logbooks.

Ship	*Time period*	*Route*
Active	Jan 1876–Nov 1878	St. Helena – East London – Natal
Barracouta	Mar 1876–Jan 1877	Fiji – Sydney – Mauritius – Simon's Town/Cape Town – St. Helena
Boxer	Jan–Dec 1878	Cape Coast – Cape of Good Hope – Cape Coast
Contest	Jan–Jul 1876	Fernando Po – Simon's Town/Cape Town – Cape Coats
Emerald	Aug 1877–Dec 1878	England – Cape of Good Hope – Australia
Encounter	Feb 1876–Nov 1877	Cape of Good Hope – Caribbean – Halifax
Frolic[a]	Apr 1876–Dec 1877	Hong Kong – Shanghai – Nagasaki
Himalaya	Jan 1877–Dec 1877	Port Said – Singapore – East London – England
Immortalite	Jan–May 1877	Sunda Strait – Mauritius – Simon's Town/Cape Town – St. Helena
Industry	Apr 1877–Dec 1878	England – Cape of Good Hope – Zanzibar – Cape of Good Hope – Accra
Magpie	Jul–Dec 1876	Plymouth – Cape of Good Hope – Singapore
Mallard	Jan 1877–May 1878	S. Helena – Sierra Leone
Narcissus	Jan 1877–May 1877	Singapore – Cape of Good Hope – England
Orontes	Jan–Oct 1877	Trincomalee – Singapore – Durban – England – Simons Bay – England
Sapphire	Feb 1877–Dec 1878	Auckland – Sydney – Hobart – Fiji – Tonga
Sirius	Jan–Sep 1876	Ascension Island – Cape of Good Hope – Fernando Po
Spiteful	Jul–Dec 1876	Gabon – Congo – Simon's Bay/Cape Town – St. Helena
Swallow	May 1877–Dec 1878	Cape Coast – River Congo – St. Helena
Tourmaline	Nov 1876–Jul 1877	Madeira – Simon's Town/Cape Town – Sierra Leone
Wolverine	Aug 1876–Jan 1877	England – Cape of Good Hope – Perth – Sydney – Fiji

[a]Daily extremes.

data points; Table 1 and Figure 1). The data typically include two daily measurements (morning and afternoon) and the geographical coordinates at noon (Figure 2), which we interpolated to the measurement times. We reduced the pressure measurements to standard gravity and to sea level by assuming a barometer elevation between 1 and 7m, depending on the ship's type, class and size. We also assumed that the pressure readings were already reduced to 0°C, although this was not indicated explicitly on the original data sheets (an attached temperature of the barometer was not provided). Data were formatted to an internationally recognised format (International Maritime Meteorological Archive (IMMA) format; Smith *et al*., 2022) and also include digitised station data from Maputo (Mozambique). All data were submitted to the Copernicus Climate Change Service data repository (GLAMOD; Noone *et al*., 2021).

In addition, we use land-based measurements from Cape Town (Royal Astronomical Observatory; Picas *et al*., 2019; Ndebele *et al*., 2020), Pietermaritzburg (Fort Napier; Allan *et al*., 2011), Port Elizabeth (Peterson and Vose, 1997) and Ribe (Kenya; Allan *et al*., 2011), as well as documentary records. The documentary records are extracted from the most comprehensive global collection available to date (Burgdorf, 2022; Burgdorf *et al*., 2022, 2023); for Africa, most of the records are semi-quantitative combinations of proxy and rain gauge data described in Nicholson *et al*. (2012). We also analyse precipitation data from a monthly gridded reconstruction based on an offline data assimilation technique (EKF400v2; Valler *et al*., 2022), from the Twentieth Century Reanalysis version 3 (20CRv3; Slivinski *et al*., 2019) and from the Global Precipitation Climatology Project Climate Data Record version 2.3 (GPCP; Adler *et al*., 2016).

Study region

Southern Africa (Figure 3) is defined by high spatiotemporal rainfall variability and recurrent wet–dry spells. Given that South Africa is located in the subtropics, the region is strongly influenced by the descending branch of the Hadley cell, thus causing generally dry conditions (Tyson and Preston-Whyte, 2000; Mahlobo *et al*., 2019). During austral summer, the southern subtropical circulation breaks up into subtropical highs located over the oceans, with monsoon-like troughs over land in-between them, and hence feeding in moisture overland (Vigaud *et al*., 2009).

In contrast with other parts of southern Africa, the westernmost region of the south-western Cape has a Mediterranean type of climate where >60% of rainfall is received during austral winter (i.e. WRZ) (Mahlalela *et al*., 2019). Here, most of the annual rainfall is associated with extratropical cyclones and occasional cut-off lows (Singleton and Reason, 2007; Mahlalela *et al*., 2019). Inter-annual rainfall variability over the WRZ is thus largely controlled by inter-annual latitudinal shifts (equatorward vs poleward) of westerly perturbations. These displacements, in turn, are influenced by a combination of factors such as sea ice anomalies in the polar southern Atlantic Ocean (Blamey and Reason, 2007) and large-scale climate modes such as ENSO (Reason and Rouault, 2002; Philippon *et al*., 2012) and the Southern Annular Mode (Lim *et al*., 2016).

Abnormal low-level divergence over the subcontinent during an El Niño and a related anomalous high pressure in the troposphere generally prevents the advection of moisture onto the continent and can result in drought (Dieppois *et al*., 2016). However, not all El Niño events necessarily result in dry conditions (e.g. South Africa did not experience particularly dry conditions during the strong 1997–1998 El Niño event) (Crétat *et al*., 2012). The relationship between ENSO and South Africa's rainfall variability is strongest during austral summer months when it peaks in amplitude (Crétat *et al*., 2012; Dieppois *et al*., 2016). This relationship also varies spatially, with the strongest influence over north- and south-eastern regions of the country (Richard *et al*., 2001; Nash and Endfield, 2008). The relationship between ENSO and rainfall variability is more complex in the WRZ. Although strong El Niño events may at times be linked to higher rainfall anomalies over the WRZ during austral winter (Philippon *et al*., 2012)

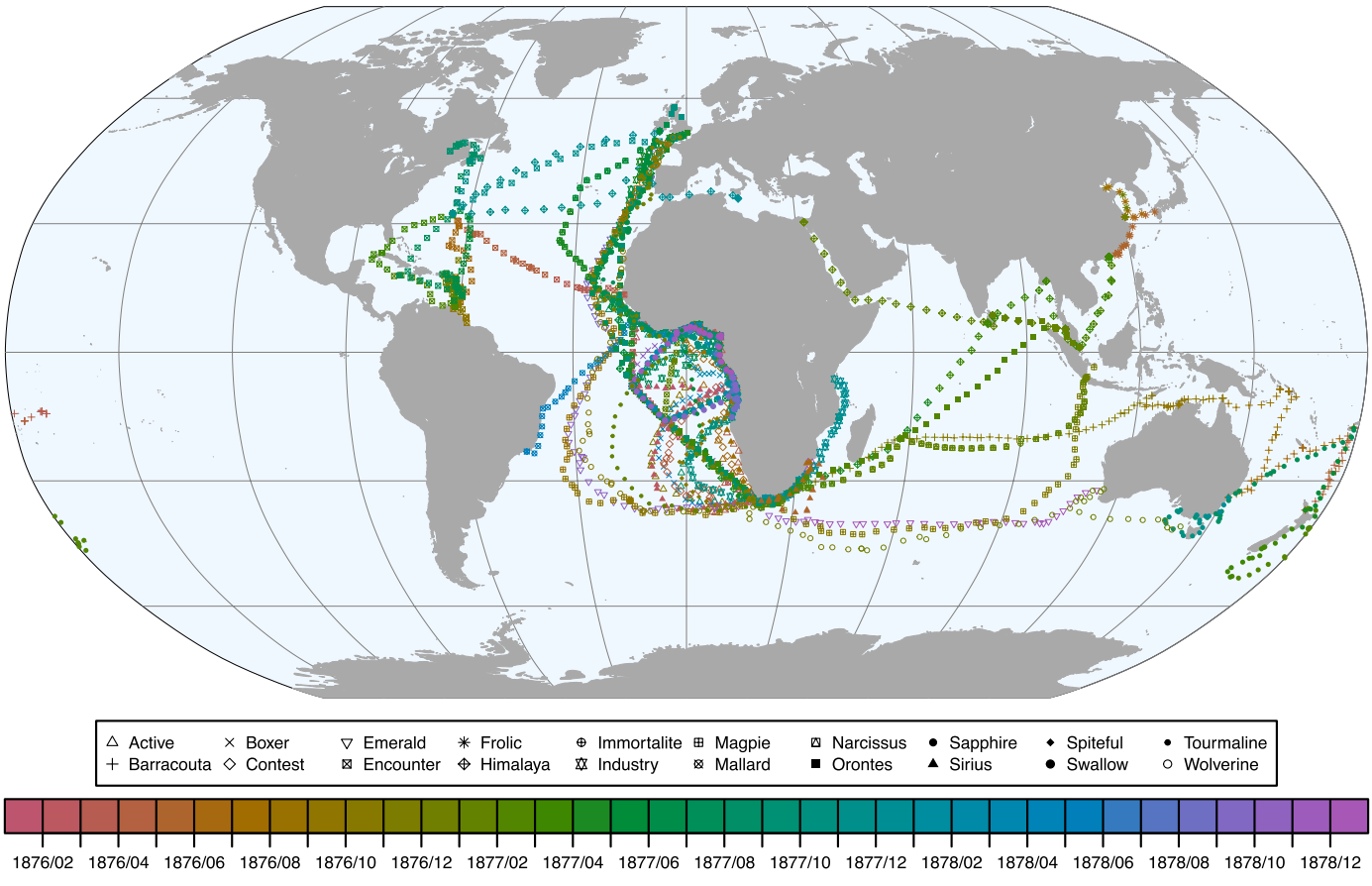

Figure 1. Tracks of the ships whose logbooks were digitised. Colours indicate the date.

and establish rainfall dipoles with the summer rainfall region (Vogel, 1989), the signal is not as strong as that during austral spring and summer seasons when ENSO phases 'mature' (Mahlalela *et al*., 2019). Hence, drought events do not necessarily affect all of southern Africa at the same time (e.g. Neukom *et al*., 2014; Singh *et al*., 2018).

Methods

20CRv3 is a global dynamical reanalysis reaching back to 1806. It consists of an ensemble of 80 members with a spatial resolution of 1°×1°. In addition to sea-surface temperatures – implicitly included in the form of boundary conditions for the numerical weather model – the only observations assimilated in 20CRv3 are pressure data, which are very scarce particularly in the Southern Hemisphere during the nineteenth century. We can improve its performance over South Africa by assimilating the newly digitised marine and land data using an offline assimilation method (i.e. the underlying numerical model simulation is not rerun) based on the Ensemble Square Root filter (for more details, see Brönnimann, 2022). We call the result 'augmented' reanalysis. Unlike the original reanalysis, we assimilate both air pressure and temperature data, and our output includes only those two variables (note that we cannot derive precipitation or any prognostic variable). Here we consider only fields at 1200 UTC and we assimilate, for each ship or station and each day, only the measurement that is closer to 1200 UTC.

Prior to assimilation, all observations were debiased relative to 20CRv3. This debiasing minimises the effects of systematic differences and preserves the 20CRv3 annual cycle and the seasonal mean spatial patterns, while the assimilated observations add intra-seasonal variability in time and space. The improvements can be evaluated with a leave-one-out cross validation approach (Figure 4), which shows an increase in the correlation between the reanalysis and the observations, particularly where no data had been assimilated in the original 20CRv3.

Precipitation anomalies during 1877–1878 in South Africa

The El Niño episode of 1877–1878 was initiated with a shift in the Southern Oscillation towards its negative phase already in late 1876 (Kiladis and Diaz, 1986), and by January 1878, the El Niño episode reportedly reached its maximum strength (Aceituno *et al*., 2009). As already mentioned, precipitation in South Africa during 1877–1878 saw contrasting anomalies between the WRZ and the SRZ. This is shown in detail in Figure 5, where data from EKF400v2 and 20CRv3 are compared with documentary records, and further explored in Figure 6 (top panel), showing the monthly precipitation anomalies in Cape Town and Port Elizabeth.

The annual precipitation in Cape Town (WRZ) in 1877 and 1878 was respectively the sixth highest and the second highest for

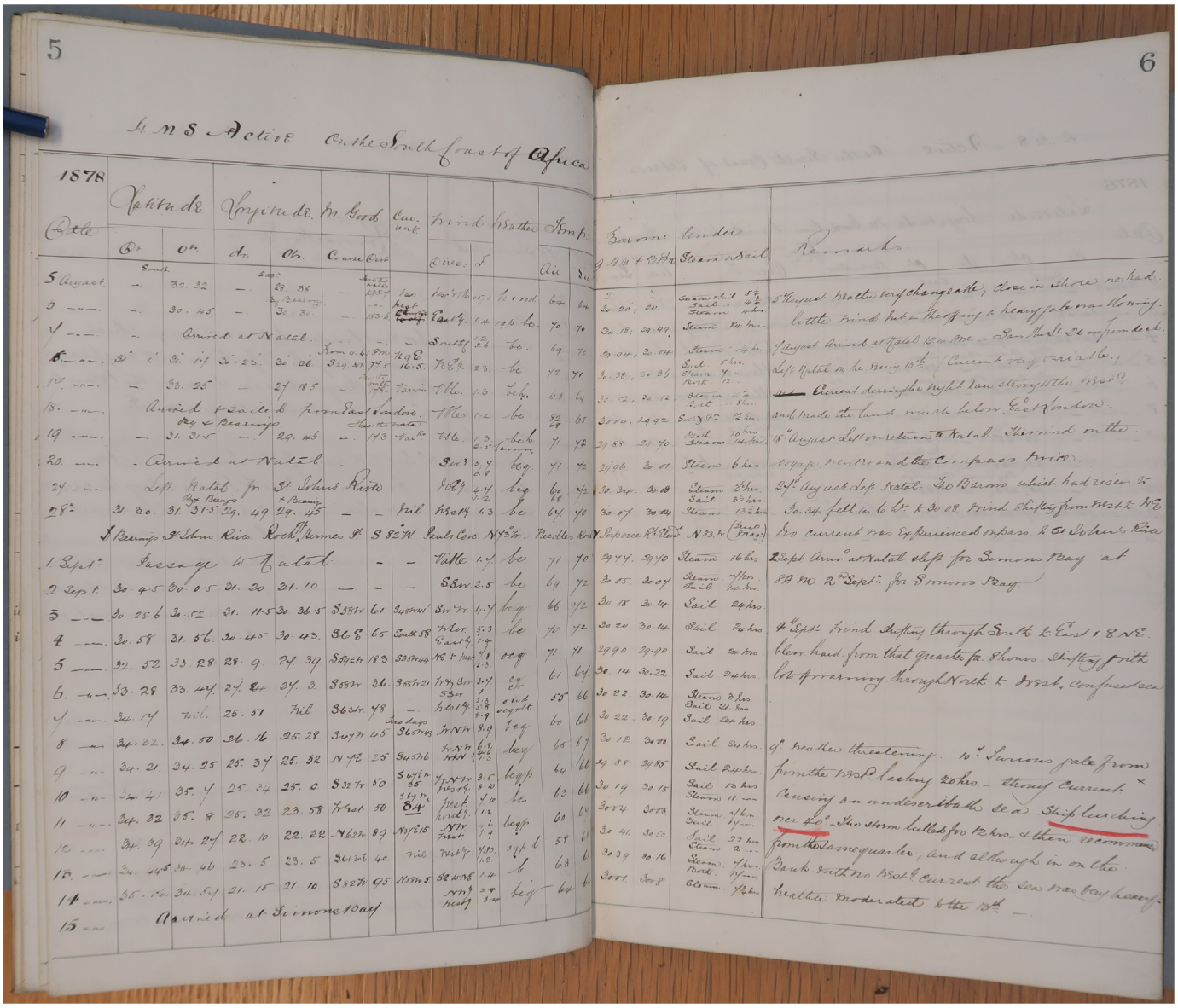

Figure 2. Example of original data sheet for HMS Active. (Source: UK Hydrographic Office.)

Figure 3. Southern Africa including provinces of South Africa and stations mentioned in the text.

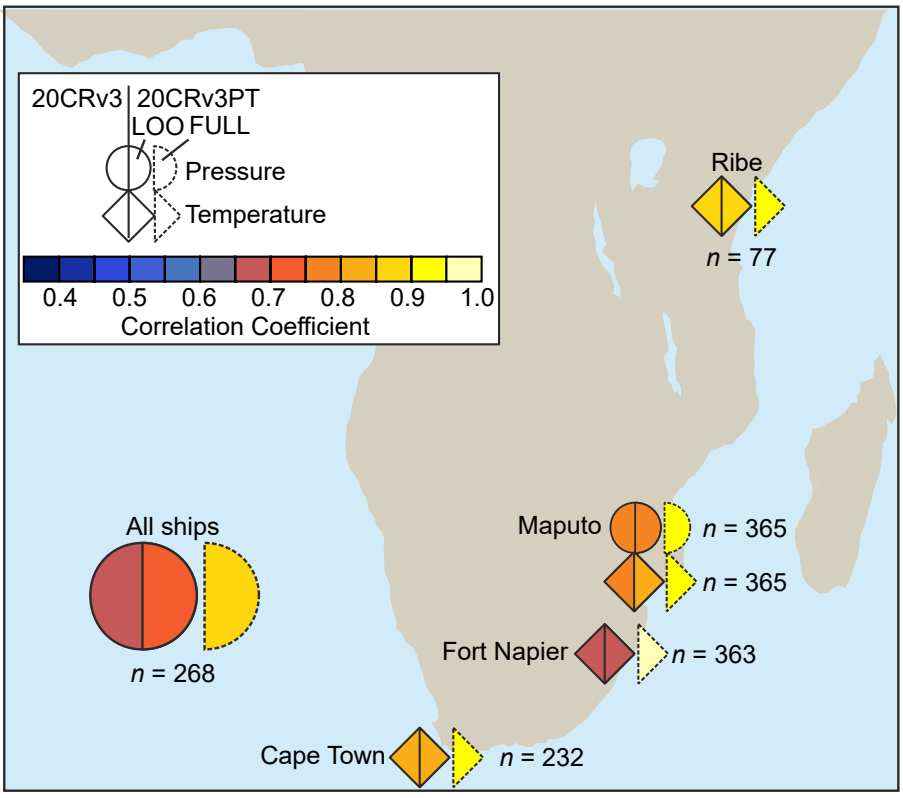

Figure 4. Spatial map of the improvement (in terms of correlation) when assimilating additional historical ship and land station data into 20CRv3. The left symbols show correlations between historical data and 20CRv3, the middle symbols show correlations with 20CRv3 augmented in a leave-one-out approach (LOO), right symbols show correlations with 20CRv3 augmented with all data assimilated (FULL). All ship observations are taken together in one symbol. The numbers indicate the observation pairs used for each correlation. The correlations are for the period July 1877–June 1878. (After Brönnimann, 2022.)

the period 1841–2016. The largest anomaly was measured between May and October 1878, when total precipitation was 75% above the long-term average (Figure 6). This extreme anomaly (corresponding to over 2mmd^{-1}) is strongly underestimated in EKF400v2 and is not reproduced at all in 20CRv3 (Figure 5), pointing to an insufficient amount of data assimilated in those products, even though several precipitation data series from South Africa are assimilated into EKF400v2.

Port Elizabeth lies at the periphery between the WRZ and SRZ, thus rainfall is more equally distributed over the year, although still slightly higher in winter. Here, negative precipitation anomalies dominated during 1877–1878 and were particularly persistent between March and September 1877 (~−60% or −1mmd^{-1} on average, the second driest such period in over a century). Again, they are better captured by EKF400v2 (which is not independent from observations), while 20CRv3 reproduces the anomaly mainly over the ocean. The precipitation deficit in Port Elizabeth continued until June 1878, with a notable wet break in October 1877 (Figure 6). The interior regions and the eastern coast experienced significant drought during both years, as indicated by documentary records and EKF400v2 (Figure 5).

In addition to the spatial contrast, there were also strong interannual differences between 1877 and 1878, in particular for the WRZ during winter. Here an extremely wet May was followed by negative precipitation anomalies during the June–September period in 1877, while positive anomalies characterised the whole winter of 1878. We can summarise the different atmospheric circulation during the two winters by analysing the average storm track through a 'storminess' index (Figure 7) – defined as the standard deviation of the daily (1200 UTC) sea-level pressure filtered with a 2–6 day Lanczos bandpass filter (Brugnara *et al.*, 2015). There was a clear equatorward shift of the storm track in the winter of 1878 with respect to 1877, consistent with more precipitation in the WRZ.

The differences between the augmented and the original reanalysis are on average small, because the amount of new data assimilated is relatively modest. The correlation with the pressure series of Cape Town and Pietermaritzburg (shown for 1877 in Figure 8) is only slightly increased, also because these data series had already been assimilated in the original 20CRv3. Large differences can arise, however, in those days when critical new data are available.

In Figure 8, the very wet period of April–May 1877 in Cape Town stands out as a succession of low pressure systems crossing the region. These are not well captured by either reanalysis, resulting in the underestimation of precipitation. One notable exception is the event of 21 April 1877, that is, the first relevant low pressure system of the season, which is much better reproduced in the augmented reanalysis. The sea-level pressure field for that day is shown in Figure 9,

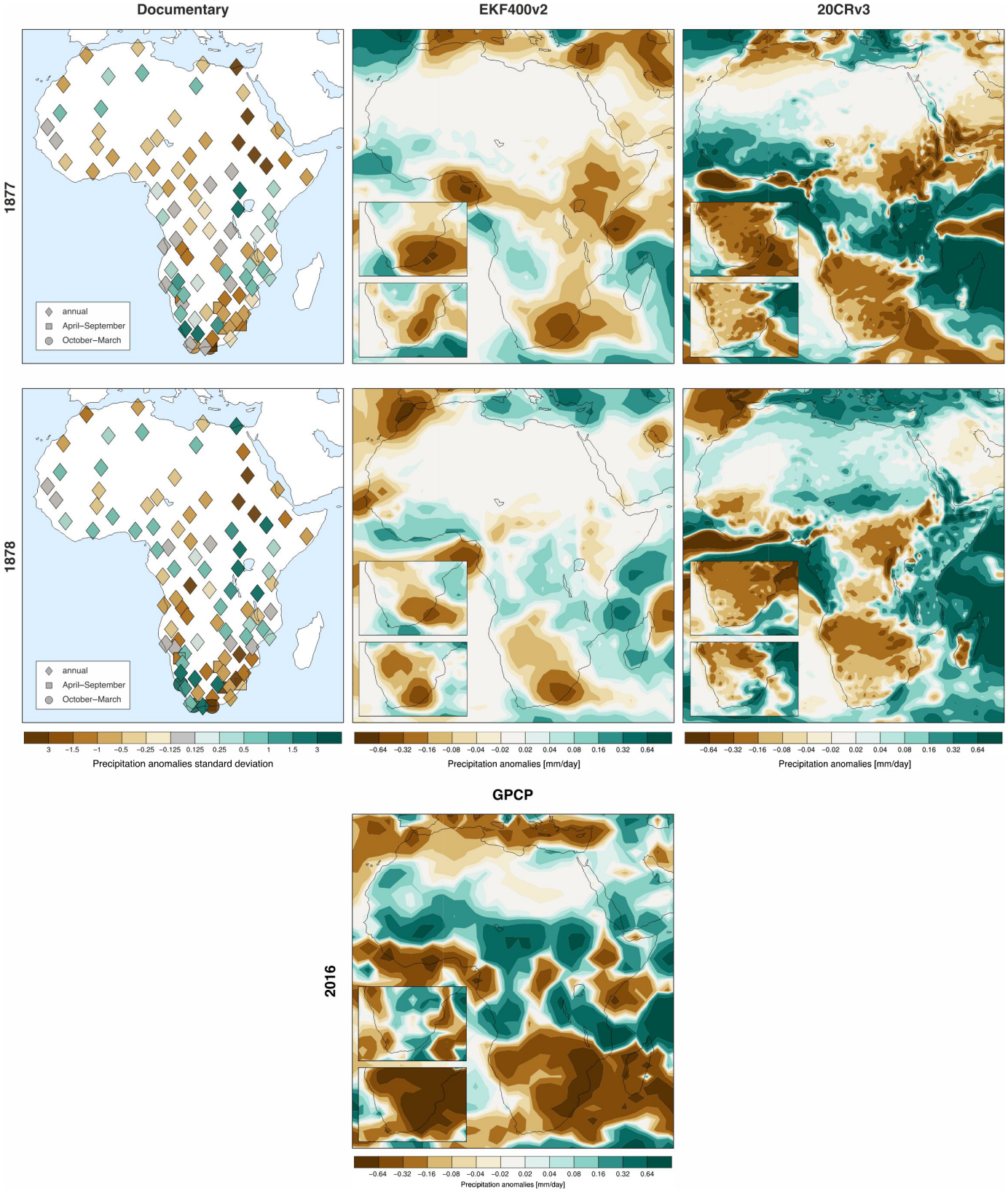

Figure 5. Annual precipitation anomalies from documentary records (Burgdorf, 2022) for 1877 (top) and 1878 (middle) with respect to the period 1867–1888 (without 1877–1878) (left panels). Anomalies that are very close to zero are coloured grey, regardless of their sign. Anomalies of annual accumulated precipitation are shown for EKF400v2 (middle panels) and 20CRv3 (right panels) for 1877 and 1878, and for Global Precipitation Climatology Project (GPCP) for 2016 (bottom). The superimposed maps indicate composites for the austral summer half-year (October 1876/1877/2015 to March 1877/1878/2016; top) and the austral winter half-year (April to September; bottom).

along with the differences between the two reanalyses. As a fortunate coincidence, three of the ships (see Table 1) were sailing not far from the pressure minimum, allowing for an accurate reconstruction of the mid-latitude cyclone in the augmented reanalysis. Our results are consistent with the strong (9.4ms^{-1}) northwesterly wind measured at Cape Town Observatory and suggest that the original 20CRv3 underestimates the pressure minimum by over 14hPa (Figure 9, bottom panel). This demonstrates the significant impact that additional marine data can have on the quality of historical reanalyses in the region.

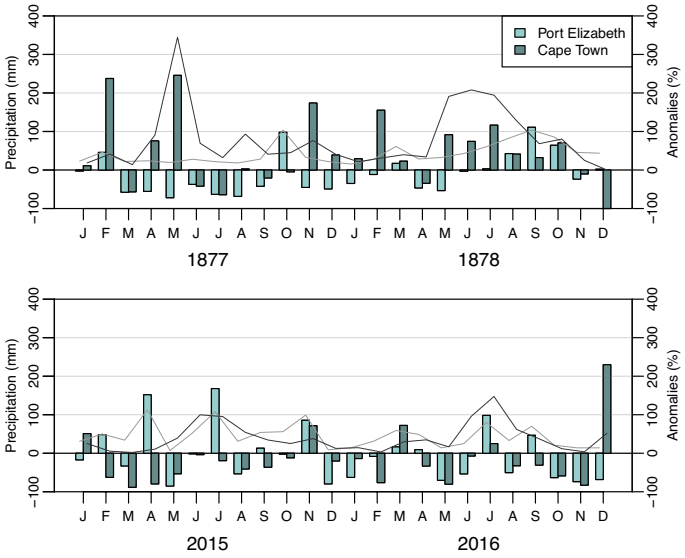

Figure 6. Total monthly precipitation (lines) and relative anomalies (bars) based off instrumental records for (top) the 1877–1878 period with respect to the 1867–1888 average (1877–1878 excluded) and (bottom) the 2015–2016 period with respect to the 1981–2010 average.

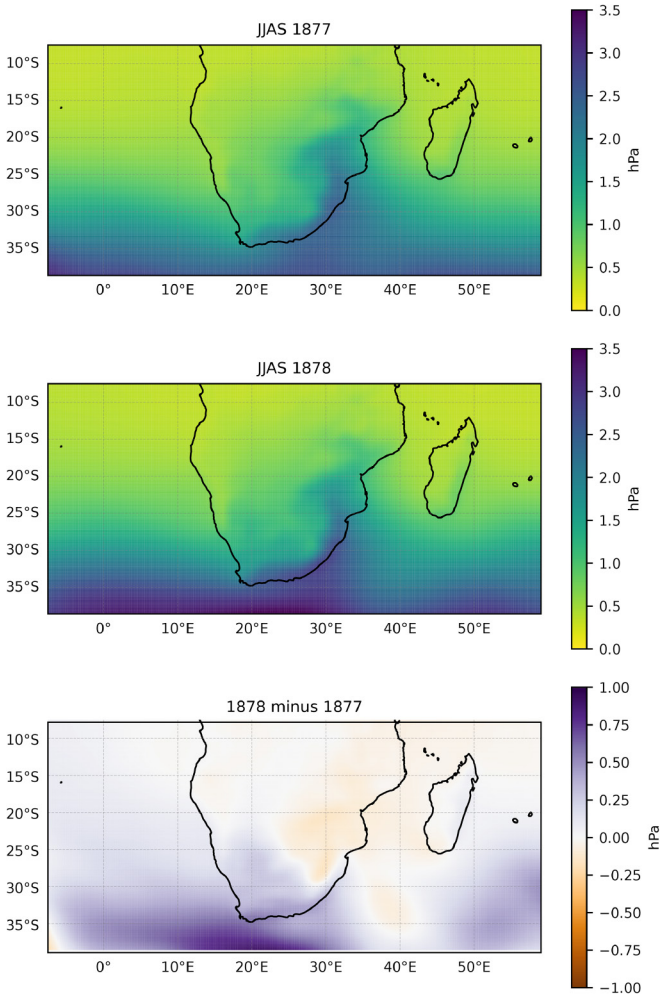

Figure 7. Maps of storminess index (standard deviation of bandpass filtered sea-level pressure) for the extended winter season (June–September) during 1877 (top) and 1878 (middle), and their difference (bottom), based on the augmented 20CRv3.

Comparison with the 2015–2016 El Niño

The most recent major El Niño event occurred between 2015 and 2016 and was comparable in magnitude to that of 1877–1878, although perhaps with different characteristics (L'Heureux *et al*., 2017). The effects on precipitation in South Africa were also different than those seen in 1877–1878, with more widespread negative anomalies concentrated in the winter half-year (Figure 5).

Both 2015 and 2016 had lower than average precipitation in Cape Town (Figure 6). The most striking differences with 1877–1878 are found in May: extremely wet in 1877 and 1878, very dry in 2015 and 2016, so that the beginning of the wet season was effectively delayed by a month. This is not entirely surprising given that the impact of ENSO on the southwestern Cape is in general highly variable and depends on many factors, such as sea-surface temperatures in the Atlantic Ocean (e.g. Mahlalela *et al*., 2019). In Port Elizabeth, negative precipitation anomalies were mainly observed during 2016 but were not as persistent as during 1877.

The 2015–16 El Niño triggered southern Africa's worst drought in 35 years (Hove and Kambanje, 2019) and a related humanitarian crisis, after which the Southern African Development Community (SADC) recommended '*strengthening of information, early warning, early action and preparedness aimed at protecting lives and livelihoods and minimizing potential impacts of disasters when they occur*' (SADC, 2016).

Conclusions

The El Niño episode of 1877–1878 triggered extreme events and persistent anomalies of opposite sign in South Africa, with exceptionally wet conditions in the Western Cape and extreme drought over the central interior and eastern provinces. Daily sea-level pressure data indicate that the anomalies involved a northward expansion of mid-latitude storm tracks during 1878, consequently resulting in an above-normal frequency of cold fronts impacting the southwestern Cape.

We have shown how data rescue can significantly improve our ability to reconstruct and better understand a past high-impact weather event such as those related to the El Niño episode of 1877–1878 – a crucial step towards better seasonal-to-decadal forecasts and more effective disaster preparedness. Unfortunately, the limited amount of data that we were able to recover was only sufficient to improve the reconstruction of single weather episodes, but did not have a large impact overall.

In the specific case of southern Africa, marine data from ships would have been particularly abundant because of the large naval traffic before the opening of the Suez Canal in 1869. Given the general absence of terrestrial instrumental weather data during such times, ship log records are invaluable for weather and climate reconstructions in such data scarce regions. However, most logbooks are still in need of being digitised

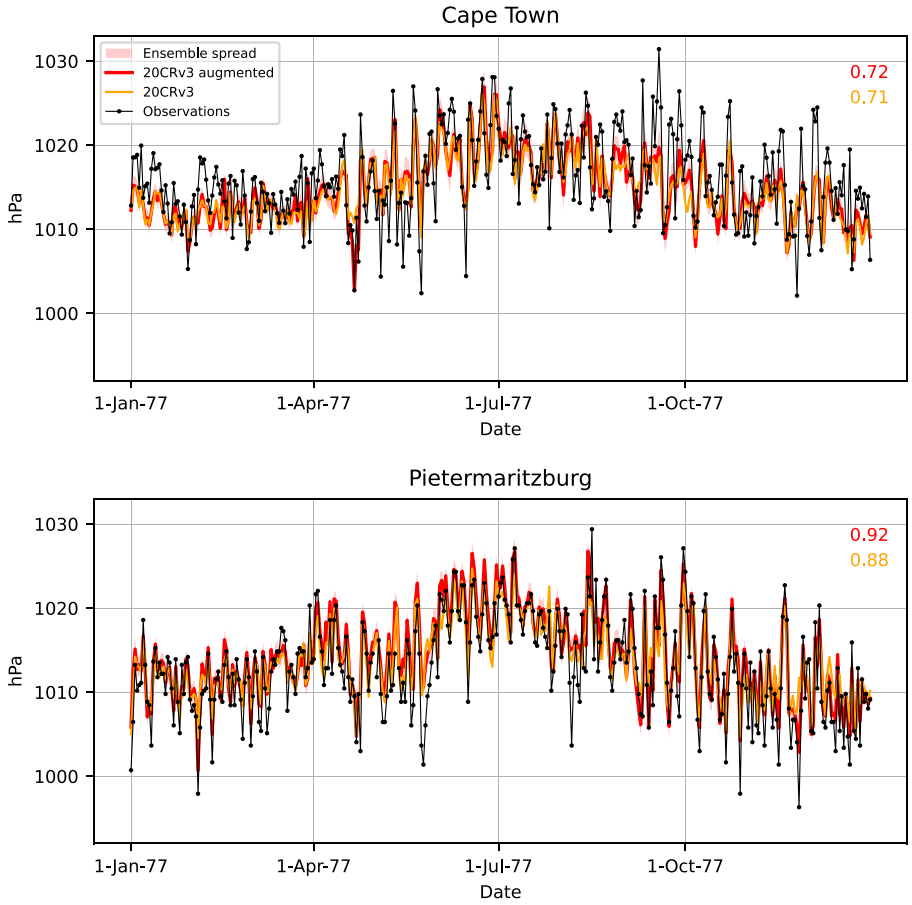

Figure 8. Sea-level pressure series observed in Cape Town (Observatory) and Pietermaritzburg (Fort Napier) during 1877, compared with the augmented and original 20CRv3. The numbers indicate the respective Pearson correlation coefficients with the instrumental series.

or have been transcribed only partially (with pressure readings having been ignored in past digitisation efforts), meaning that data rescue will remain an important component of weather and climate research in the coming years.

Acknowledgements

This work was supported by the UK Newton Fund within the framework of the Weather and Climate Science for Service Partnership (WCSSP) South Africa and by the European Commission (ERC Grant PALAEO-RA, 787574). Open access funding provided by Universitat Bern.

Author contributions

Yuri Brugnara: Writing – original draft; data curation; visualization; conceptualization; formal analysis. **Stefan Brönnimann:** Conceptualization; methodology; formal analysis; data curation; visualization; funding acquisition. **Stefan Grab:** Writing – original draft; data curation; visualization; conceptualization. **Jessica Steinkopf:** Writing – original draft; data curation. **Angela-Maria Burgdorf:** Data curation; visualization. **Clive Wilkinson:** Data curation. **Rob Allan:** Data curation; funding acquisition.

References

Aceituno P, del Rosario Prieto M, Solari ME *et al*. 2009. The 1877–1878 El Niño episode: associated impacts in South America. *Clim. Chang.* **92**: 389–416.

Adler R, Wang J-J, Sapiano M *et al*. 2016. Global Precipitation Climatology Project (GPCP) Climate Data Record (CDR), Version 2.3 (Monthly). National Centers for Environmental Information. https://doi.org/10.7289/V56971M6

Allan R, Brohan P, Compo GP *et al*. 2011. The international atmospheric circulation reconstructions over the earth (ACRE) initiative. *Bull. Am. Meteorol. Soc.* **92**: 1421–1425.

Blamey R, Reason CJC. 2007. Relationships between Antarctic sea-ice and South African winter rainfall. *Clim. Res.* **33**: 183–193.

Brönnimann S. 2022. Historical observations for improving reanalyses. *Front. Clim.* **4**: 880473.

Brugnara Y, Auchmann R, Brönnimann S *et al*. 2015. A collection of sub-daily pressure and temperature observations for the early instrumental period with a focus on the "year without a summer" 1816. *Clim. Past* **11**: 1027–1047.

Burgdorf A-M. 2022. A global inventory of quantitative documentary evidence related to climate since the 15th century. *Clim. Past* **18**: 1407–1428.

Burgdorf A-M, Brönnimann S, Adamson G *et al*. 2023. DOCU-CLIM: a global documentary climate dataset for climate reconstructions. *Sci. Data* **10**: 402.

Burgdorf A-M, Brönnimann S, Adamson G *et al*. 2022. DOCU-CLIM: A Global Documentary Climate Dataset for Climate Reconstructions [Dataset]. https://boris-portal.unibe.ch/handle/20.500.12422/207

Crétat J, Richard Y, Pohl B *et al*. 2012. Recurrent daily rainfall patterns over South Africa and associated dynamics during the core of the austral summer. *Int. J. Climatol.* **32**: 261–273.

Davis M. 2001. *Late Victorian Holocausts: El Niño Famines and the Making of the Third World*. Verso Books: London.

Dieppois B, Pohl B, Rouault M *et al*. 2016. Interannual to interdecadal variability of winter and summer southern African rainfall, and their teleconnections. *J. Geophys. Res.* **121**: 6215–6239.

Hao Z, Zheng J, Wu G *et al*. 2010. 1876–1878 severe drought in North China: Facts, impacts and climatic background. *Chin. Sci. Bull.* **55**: 3001–3007.

Hove L, Kambanje C. 2019. Lessons from the El Nino–induced 2015/16 drought in the Southern Africa region. *Curr. Dir. Water Scarcity Res.* **2**: 33–54.

Huang B, L'Heureux M, Hu ZZ *et al*. 2020. How significant was the 1877/78 El Niño? *J. Clim.* **33**: 4853–4869.

Kiladis GN, Diaz HF. 1986. An analysis of the 1877–78 ENSO episode and comparison with 1982–83. *Mon. Weather Rev.* **114**: 1035–1047.

L'Heureux ML, Takahashi K, Watkins AB *et al*. 2017. Observing and predicting the 2015/16 El Niño. *Bull. Am. Meteorol. Soc.* **98**: 1363–1382.

Lim EP, Hendon HH, Arblaster JM *et al*. 2016. The impact of the Southern Annular Mode on future changes in Southern Hemisphere rainfall. *Geophys. Res. Lett.* **43**: 7160–7167.

Mahlalela PT, Blamey RC, Reason CJC. 2019. Mechanisms behind early winter rainfall variability in the southwestern Cape, South Africa. *Clim. Dyn.* **53**: 21–39.

Mahlobo DD, Ndarana T, Grab S *et al*. 2019. Integrated climatology and trends in the subtropical Hadley cell, sunshine duration and cloud cover over South Africa. *Int. J. Climatol.* **39**: 1805–1821.

Nash D. 2017. Changes in precipitation over southern Africa during recent centuries. In: *Oxford Research Encyclopedia of Climate Science*. Oxford University Press: Oxford. https://doi.org/10.1093/acrefore/9780190228620.013.539

Nash DJ, Endfield GH. 2008. 'Splendid rains have fallen': links between El Niño and rainfall variability in the Kalahari, 1840–1900. *Clim. Chang.* **86**: 257–290.

Nash DJ, Klein J, Endfield GH *et al*. 2019. Narratives of nineteenth century drought in southern Africa in different historical source types. *Clim. Chang.* **152**: 467–485.

Ndebele NE, Grab SW, Turasie A. 2020. Characterizing rainfall in the south-western Cape, South Africa: 1841–2016. *Int. J. Climatol.* **40**: 1992–2014.

Neukom R, Nash DJ, Endfield GH *et al*. 2014. Multi-proxy summer and winter

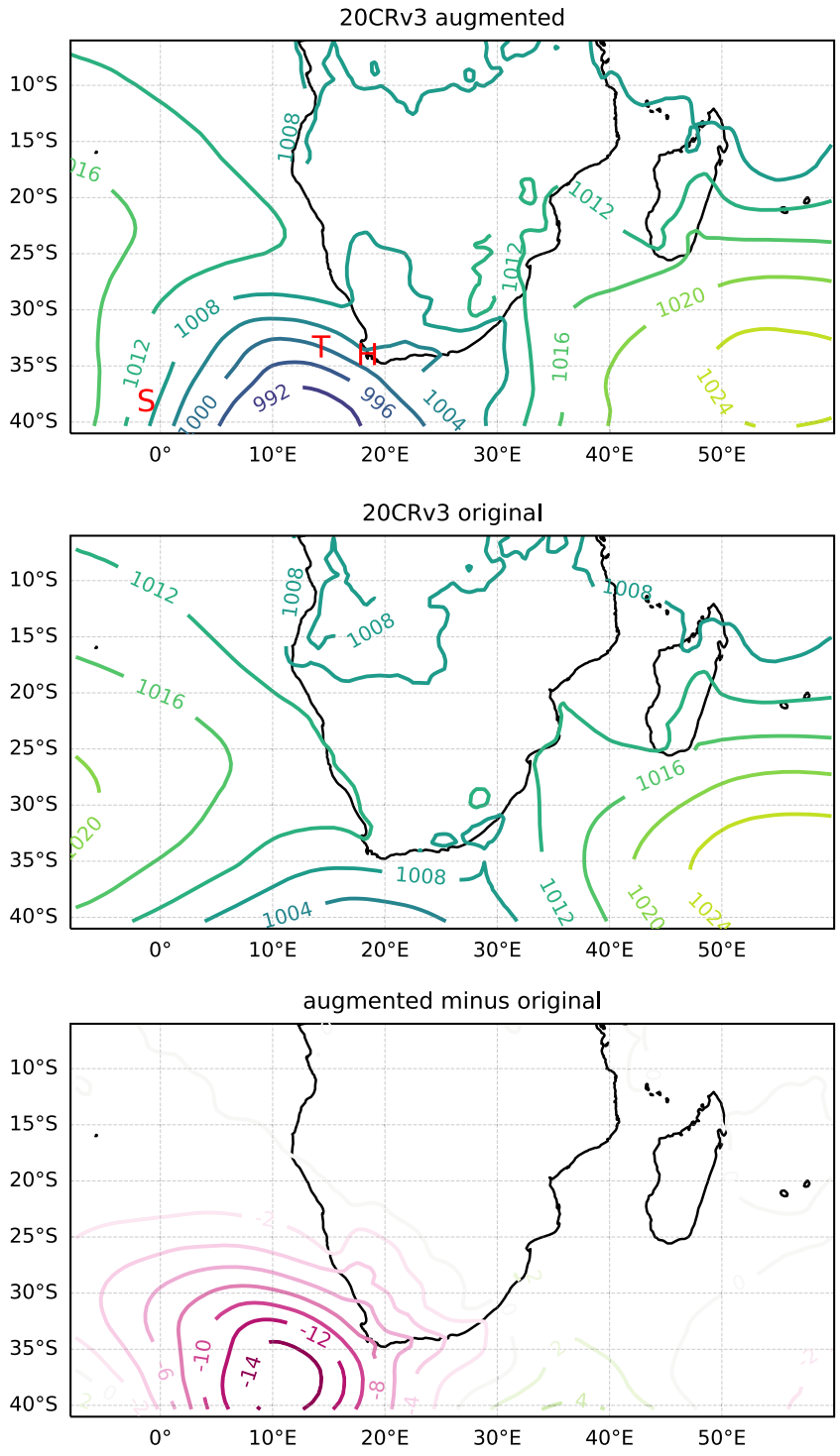

Figure 9. Sea-level pressure field (in hPa) on 21 April 1877, 1200 UTC. The letters in the top panel indicate the positions of the ships Himalaya (H), Sapphire (S) and Tourmaline (T) at local noon.

precipitation reconstruction for southern Africa over the last 200 years. *Clim. Dyn.* **42**: 2713–2726.

Nicholson S, **Klotter D**, **Dezfuli A**. 2012. Spatial reconstruction of semi-quantitative precipitation fields over Africa during the nineteenth century from documentary evidence and gauge data. *Quat. Res.* **78**: 13–23.

Nicholson SE, **Kim J**. 1997. The relationship of the El Niño–Southern oscillation to African rainfall. *Int. J. Climatol.* **17**: 117–135.

Noone S, **Atkinson C**, **Berry DI *et al***. 2021. Progress towards a holistic land and marine surface meteorological database and a call for additional contributions. *Geosci. Data J.* **8**: 103–120.

Peterson TC, **Vose RS**. 1997. Global Historical Climatology Network – Monthly (GHCN-M), Version 2. NOAA National Centers for Environmental Information. https://doi.org/10.7289/V5X34VDR

Philippon N, **Rouault M**, **Richard Y** *et al*. 2012. The influence of ENSO on winter rainfall in South Africa. *Int. J. Climatol.* **32**: 2333–2347.

Picas J, **Grab S**, **Allan R**. 2019. A 19th century daily surface pressure series for the southwestern Cape region of South Africa: 1834–1899. *Int. J. Climatol.* **39**: 1404–1414.

Reason CJC, **Rouault M**. 2002. ENSO-like decadal variability and South African rainfall. *Geophys. Res. Lett.* **29**: 16-1–16-4.

Richard Y, **Fauchereau N**, **Poccard I *et al***. 2001. 20th century droughts in southern Africa: spatial and temporal variability, teleconnections with oceanic and atmospheric conditions. *Int. J. Climatol.* **21**: 873–885.

SADC. 2016. *Regional Humanitarian Appeal June 2016.* Southern African Development Community. https://www.sadc.int/files/4814/6840/2479/SADC_Regional_Humanitarian_Appeal_June_20160713.pdf [Accessed 14 June 2022].

Singh D, **Seager R**, **Cook BI *et al***. 2018. Climate and the global famine of 1876–78. *J. Clim.* **31**: 9445–9467.

Singleton AT, **Reason CJC**. 2007. Variability in the characteristics of cut-off low pressure systems over subtropical southern Africa. *Int. J. Climatol.* **27**: 295–310.

Slivinski LC, **Compo GP**, **Whitaker JS** *et al*. 2019. Towards a more reliable historical reanalysis: Improvements for version 3 of the Twentieth Century Reanalysis system. *Q. J. R. Meteorol. Soc.* **145**: 2876–2908.

Smith SR, **Freeman E**, **Lubker SJ** *et al*. 2022. *The International Maritime Meteorological Archive (IMMA) Format*. https://icoads.noaa.gov/e-doc/imma/R3.0-imma1.pdf [Accessed 24 May 2022].

Tyson PD, **Preston-Whyte RA**. 2000. *Weather and Climate of Southern Africa*. Oxford University Press: Oxford.

Valler V, **Franke J**, **Brugnara Y *et al***. 2022. An updated global atmospheric paleo-reanalysis covering the last 400 years. *Geosci. Data J.* **9**: 89–107.

Vigaud N, **Richard Y**, **Rouault M *et al***. 2009. Moisture transport between the South Atlantic Ocean and southern Africa: relationships with summer rainfall and associated dynamics. *Clim. Dyn.* **32**: 113–123.

Vogel CH. 1989. A documentary-derived climatic chronology for South Africa, 1820–1900. *Clim. Change* **14**: 291–307.

Correspondence to: Y. Brugnara
yuri.brugnara@giub.unibe.ch

doi: 10.1002/wea.4468